

# Analysis and Design of Gyro-Drive Mode Loop with Amplitude Control

Ahmad Shaban

Si-Ware Systems,  
Cairo, Egypt.

ahmad.shaban@si-ware.com

Mohammed El-Badry

Si-Ware Systems,  
Cairo, Egypt.

mohammed.elbadry@si-ware.com

Ayman El-Sayed

Si-Ware Systems,  
Cairo, Egypt.

ayman.elsayed@si-ware.com

**Abstract**— This paper presents the system architecture of a primary mode oscillation loop of a MEMS GYRO interface. The loop is designed using an all digital PLL acting as a frequency selective gain element in the positive feedback oscillation loop. An amplitude control negative feedback loop is implemented to maintain the stability of oscillation amplitude and consequently the output reading scale factor. A new methodology for modelling the Gyro sensing element in the context of the amplitude loop is presented. System analysis based on this model is presented and verified by simulation.

**Keywords** — Vibratory gyroscope, angular velocity sensor, automatic amplitude control.

## I. INTRODUCTION

Inertial sensors, which comprise gyroscopes and accelerometers, are used to measure either the rotation rate or the acceleration of a body with respect to an inertial frame of reference [1].

MEMS gyroscopes can provide significant cost, size and weight advantages over traditional sensors. This has resulted in a proliferation of the applications in which such sensors can be used [2]. They can be used with MEMS accelerometers to provide information for inertial navigation purposes, automotive applications for ride stabilization and rollover detection as well as some consumer electronics applications [3].

Fig. 1 shows a typical MEMS gyroscope [6]. It relies on a mechanical structure that is driven into resonance in one axis and excites a secondary oscillation due to Coriolis force in another perpendicular axis. The amplitude of the secondary oscillation is directly proportional to the angular rate signal to be measured  $\Omega$  [4]. The expression for Coriolis force  $F_{cor}$  is given in (1), where  $m$  is the proof mass,  $v_r$  is the velocity of the primary mode oscillation and  $\vec{a}_{cor}$  is the Coriolis acceleration.

$$\vec{F}_{cor} = 2 \cdot m \cdot \vec{\Omega} \times \vec{v}_r = m \cdot \vec{a}_{cor} \quad (1)$$

The stability of the amplitude and frequency of the drive mode oscillation is essential as they determine the scale factor of the sensor reading. A typical architecture for a digital drive loop uses a PLL in the feedback as in [5].

In addition to presenting the system-level architecture and the implementation of the gyro primary mode oscillator using an all digital PLL, a linearized model of the gyro effect on the oscillation amplitude is for the analysis and design of the amplitude control loop.

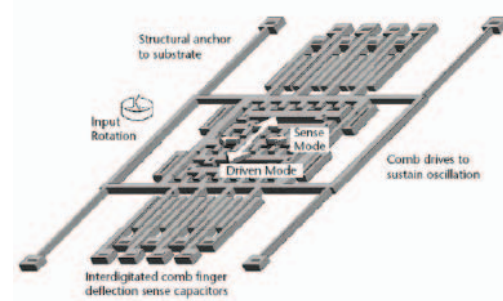


Fig. 1 MEMS Gyroscope of [6].

In Section II, the different blocks that form the system are described. In Section III, the architecture of the primary mode oscillation loop is explained showing merits of the PLL. Section IV describes the design of automatic amplitude control loop necessary for obtaining stable oscillations as well as simulation results for the complete loop. Finally, the paper is concluded in Section V.

## II. SYSTEM OVERVIEW

The gyroscope sensor system; shown in Fig. 2 is built of three parts that work together. These parts are a micromechanical sensor element, analog circuitry and digital signal processing.

### A. Analog Circuitry

The analog blocks in the system include the actuation DACs to drive the primary mode oscillation, as well as the gyro front end detection circuits which include capacitance to voltage converter (C/V) and ADC for digitization. The design of these blocks is beyond the scope of the paper.

### B. Digital Processing

This includes the drive loop blocks, detection and actuation interfaces as well as the sense interface and the demodulation necessary to obtain the angular rate reading which is modulated on the primary mode carrier as explained in Section I.

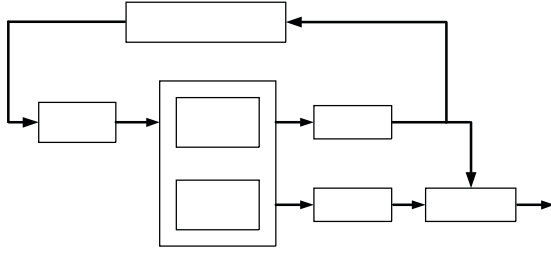


Fig. 2 Block Diagram for the gyroscope sensor system.

### III. DRIVE MODE OSCILLATION LOOP

The drive mode loop is a positive feedback loop responsible for maintaining sustained oscillation in the primary mode of the MEMS gyro.

For a feedback system as the one shown in Fig. 3 the Barkhausen criteria for a stable oscillation requires the gain around the loop to be equal or greater than unity, also a phase condition is necessary which implies that the phase around the loop is equal to zero or  $2n\pi$  as shown in (3).

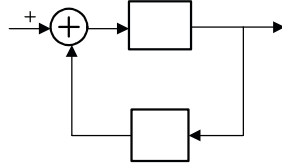


Fig. 3 Feedback System.

$$\frac{V_o(s)}{V_{in}(s)} = \frac{A(s)}{1 - \beta(s).A(s)} \quad (2)$$

$$\angle(\beta(s).A(s)) = 2n\pi \quad \text{Where, } n = 0, 1, 2, \dots$$

$$|\beta(s).A(s)| \geq 1 \quad (3)$$

The gyro displacement in the drive axis is a second order function of the applied electrostatic actuation force as given in (4); where  $m$  is the proof mass,  $\omega_d$  and  $Q_d$  are the drive mode resonance angular rate and quality factor respectively. Bode plot of the transfer function is plotted in Fig. 4.

$$\frac{x(s)}{F(s)} = \frac{1/m}{s^2 + \frac{\omega_d}{Q_d}s + \omega_d^2} \quad (4)$$

As shown in Fig. 4 the gyro causes a phase shift of  $-90^\circ$  to the input actuation force at resonance. The loop must exhibit a  $+90^\circ$  (or  $2n\pi + \pi/2$ ) phase shift to achieve the oscillation condition. An all digital PLL is used to get the appropriate phase shift to close the positive feedback loop as shown in Fig. 5. The PLL, as shown, consists of a Phase Frequency Detector (PFD) that detects the zero crossings of the input and feedback signals, a digital low pass filter and a Direct Digital Synthesizer (DDS). The phase condition around the loop is achieved by taking the appropriate phase from the DDS output

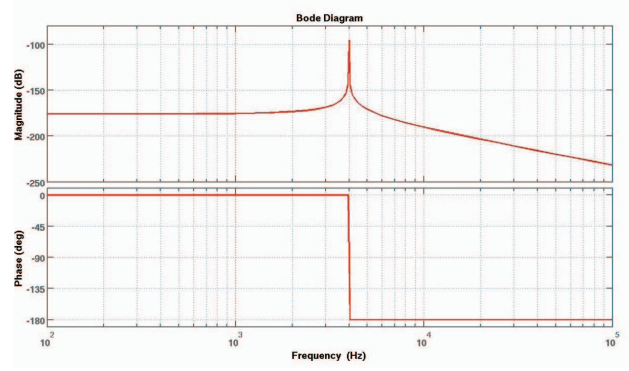


Fig. 4 Bode Plot of the gyro drive mode response for  $\omega_d = 2\pi \cdot 4$  KHz and  $Q_d = 1e4$ . Plot is normalized on  $1/m$ .

with certain phase shift ( $\Delta\phi$ ) from the input signal to the PLL.

The PLL can be considered as an infinite gain block in the oscillation loop. It resolves zero crossings of the input signal and outputs fixed amplitude oscillations. The necessary requirement is that the gain in the loop from the PLL output back to the PFD input is enough to have the signal above noise margin of the PFD in order to correctly detect the phase.

Quantization noise at the PFD inputs can be reduced by increasing the sampling rate [7]. This quantization noise shall be filtered by the PLL loop filter. The DDS quantization noise can be minimized by increasing the number of bits at its output and reducing phase quantization at the control input.

The DDS has a limited range for its output frequency; this is equivalent to limiting the gain condition of the positive feedback loop to this range of frequencies. The loop can not build oscillation at a frequency outside this range. This property is very useful for the drive oscillation loop; it prevents excitation of undesired oscillation modes of the MEMS by diminishing the loop gain at these frequencies.

The PLL architecture also allows obtaining a synchronous clock locked with the drive oscillation which would be useful for SD force feedback solution for the sense mode of the gyro [5, 8].

### IV. AUTOMATIC AMPLITUDE CONTROL - AAC

The function of the AAC is to maintain drive mode mechanical oscillations of the gyro at fixed amplitude. This is done by setting the amplitude of the oscillation voltage signal by a negative feedback loop. The loop is desensitized to electrostatic actuation constants as well as quality factor of the gyro drive mode, whereas it is sensitive to the motion to capacitance constants and the gain of the C/V front end.

In order to control the oscillation amplitude, the AAC extracts amplitude information from the oscillation signal and feeds back control signal to set the amplitude. In that manner, the oscillation signal can be considered as an AM signal with carrier frequency equal to the drive mode oscillation frequency. The AAC loop acts on the envelope which is the modulating signal.

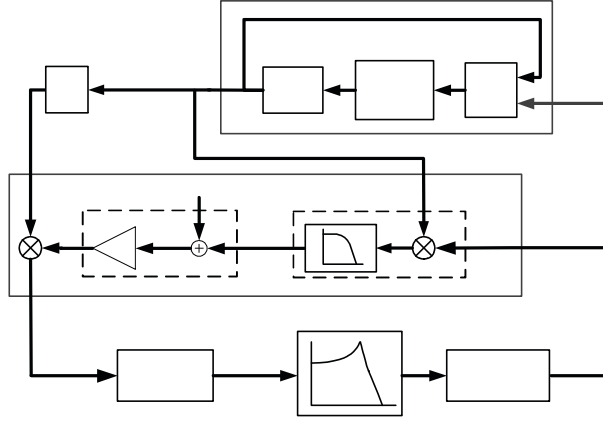


Fig. 5 Detailed block diagram for the drive loop.

#### A. Peak Detection

A common method for peak detection extracts the amplitude by squaring the signal where low frequency output represents the amplitude information; however this method introduces non-linearity because its output is proportional to the square of the amplitude.

In this design the DDS output is used for synchronous demodulation of the input signal as shown in Fig. 5. The amplitude information is down converted to low frequency. Since, the PLL output has a fixed amplitude independent on input signal amplitude, the detected peak is linearly proportional to the amplitude of the input signal.

#### B. Infinite Impulse Response(IIR) – 4<sup>th</sup> order Butterworth

Sufficient suppression of the 2<sup>nd</sup> harmonic is necessary, in order to avoid contamination of actuation signal with undesired tones due to mixing. These undesired tones would couple through the gyro to the detection circuitry and increase noise of output oscillation. A 4<sup>th</sup> order IIR-Butterworth filter was used with cut-off at 100Hz.

In implementation of the filter, the number of bits used for adders and multipliers inside the filter should be well optimized to avoid oscillation of the filter, as such IIR filter contains internal feedback which may oscillate due to increased quantization noise injected at internal nodes.

#### C. GYRO Model for AAC Loop

The MEMS gyro is modelled as a second order system as explained in Section III; this model is valid for the input signal. However, for the AAC loop we are concerned with the response of the gyro to input signal at resonance with varying amplitude.

As described above the signal propagating in the AAC is the amplitude signal, the transfer function required for the gyro can be obtained by studying the response of the gyro to the envelope of input amplitude modulated (AM) signal with its carrier frequency at the gyro drive mode resonance. The input test signal  $V_{in}(t)$  is given by (5), where  $\omega_m$  is the angular rate of the modulating signal and  $A_d$  is the amplitude of the carrier.

The three components of the input signal pass through the gyro and each acquires a certain phase shift and gain according to the transfer function in (4).

$$\begin{aligned} V_{in}(t) &= (A_d + \sin(\omega_m t)) \cdot \sin(\omega_d t) \\ &= A_d \sin(\omega_d t) + \frac{1}{2} \cos((\omega_d - \omega_m)t) - \frac{1}{2} \cos((\omega_d + \omega_m)t) \end{aligned} \quad (5)$$

Assuming small value of  $\omega_m$ ; the gyro response to both sidebands can be considered symmetric about the carrier frequency. The output signal from the gyro  $V_o(t)$  is given in (6). Due to symmetry of the side bands around the resonance frequency, the phase shifts acquired by these two components  $\phi_1$  and  $\phi_2$  have a certain relation represented in (7).

$$\begin{aligned} V_o(t) &= -A'_d \cos(\omega_d t) + \frac{a}{2} \cos((\omega_d - \omega_m)t + \phi_1) \\ &\quad - \frac{a}{2} \cos((\omega_d + \omega_m)t + \phi_2) \end{aligned} \quad (6)$$

$$\text{If } \phi_1 = -\theta \text{ then } \phi_2 = \theta - 180^\circ \quad (7)$$

For the case of high quality factor gyro ( $>1e2$ ) and low resonance frequency (few KHz), the phase step is sharp, so  $\theta$  is almost equal zero degrees. The output AM wave will have its envelope  $-90^\circ$  shifted from the envelope of the input as shown in (8). The gain acquired by the envelope exhibits almost the same characteristic roll-off of the gyro gain at resonance due to the high quality factor.

$$V_o(t) \approx -(A'_d + a \cos(\omega_m t)) \cdot \cos(\omega_d t) \quad (8)$$

The above discussion describes the required transfer function as  $-90^\circ$  shift for the phase response, while the amplitude response is similar to gyro roll-off shifted to DC. Such response can not be easily modelled in the s-domain. The gyro response for the amplitude signal is approximated to a single pole system with the pole located at its BW ( $\omega_d / Q_d \approx 2\text{Hz}$  for  $\omega_d = 2\pi * 4 \text{ KHz}$  and  $Q_d = 1e4$ ). The AAC loop is designed as dominant pole system which is the gyro, this means that assuming the gyro roll-off as 20dB/dec represents worst case phase margin, the actual loop gain roll-off ensures better phase margin for the AAC loop.

#### D. Amplitude Control Block

The control block as shown in Fig. 5, subtracts the peak signal output of the peak detector from the desired reference amplitude setting. The error is then amplified and fed back to the gyro input. The AAC loop in that way incorporates a proportional controller. The steady state error is inversely proportional to the loop gain.

The linear model of the AAC contains a single pole of the gyro and 4 poles of the IIR filter. Due to the low resonance frequency and high quality factor of the gyro, the gyro pole is considered the dominant pole. In determining the proportional gain  $P_g$  of the AAC, there is a clear trade off between stability in one side and steady state error as well as settling time on the other side. As the value of the proportional gain increases the

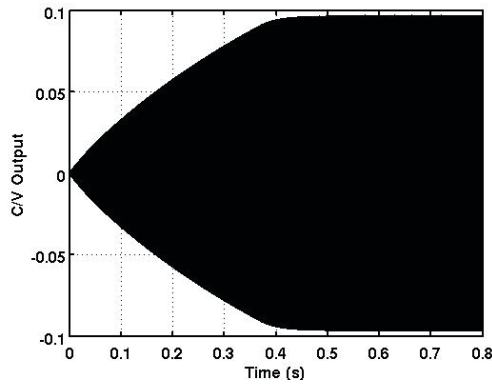


Fig. 6 Drive Loop Oscillation start-up.

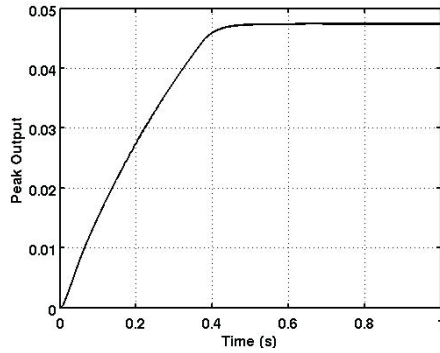


Fig. 7 Output of the peak detection block.

steady state error decreases and so does the settling time of the AAC, however the phase margin decreases too.

#### E. Simulation Results

The complete system is simulated on Simulink™. Fig. 6 shows the waveform of the output oscillation during start-up. The start-up time depends on the target amplitude by the AAC as well as the initial frequency shift of the PLL centre frequency from the gyro drive resonance in addition to quality factor of the gyro drive mode. Fig. 7 shows the output from the peak detection block, the detected peak is equal to that of the signal but divided by a factor of 2 due to synchronous demodulation method. The AAC control line which is the output of the amplitude control block is shown in Fig. 8. The value of the control line remains at its maximum value during start-up. After oscillation build up, the control line decays to its final value. The decay of the AAC control line as well as the growth of the peak output does not exhibit overshoots.

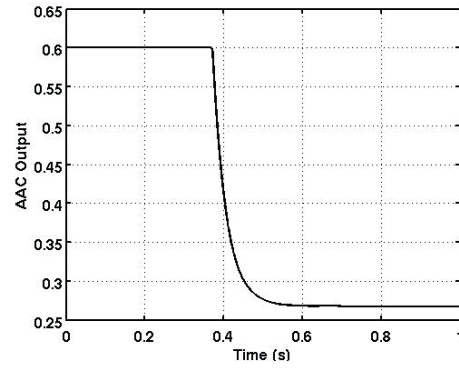


Fig. 8 AAC Output control line

#### V. CONCLUSIONS

The system level architecture of gyro drive mode loop is presented. Amplitude control loop with linear peak detection is proposed. Modelling of the gyro effect on the signal amplitude is studied and a new linearized model is introduced. The design methodology is verified by time domain simulations of the complete loop. Excellent loop stability, oscillation start up and amplitude locking characteristics are demonstrated.

#### ACKNOWLEDGMENT

The authors wish to acknowledge Bassel Hanafi, B. Zaki and A. Mokhtar at Si-Ware systems for their useful discussions.

#### REFERENCES

- [1] Mikko Saukoski, *Systems and Circuit Design for a Capacitive MEMS GYROSCOPE*. PhD thesis, Helsinki University of Technology, 2008.
- [2] N. Barbour & G. Schmidt. *Inertial sensors technology trends*. IEEE Sensors Journal, vol. 1, no. 4, pages 332 – 339, Dec. 2001.
- [3] F. Ayazi N.Yazdi & K. Najafi. Micromachined inertial sensors. In *Proceedings of the IEEE*, volume 86, pages 1640 – 1659, Aug., 1998.
- [4] Michael Kraft Stephen Beeby Graham Ensell & Neil White. *MEMS Mechanical Sensors*. Artech House, 2004.
- [5] Mikko Saukoski, Lasse Aaltonen, Teemu Salo and Kari Halonen, "Readout and Control Electronics for a Microelectromechanical Gyroscope", IMTC, April 2006.
- [6] R. T. Howe Clark W. A. & R. Horowitz. Surface Micromachined Z-Axis Vibratory Rate Gyroscope. In *Digest of Solid-State Sensors and Actuator Workshop*, pages 283–287, 1996.
- [7] J. Belzile and N. Batani, "Low phase noise programmable clock generators for wireless modems", SPAWC '99.
- [8] L. Aaltonen, M. Saukoski, and K. Halonen, "Design of Clock Generating Fully Integrated PLL Using Low Frequency Reference Signal", *Proc. Eur. Conf. on Circuit Theory and Design*, Vol. I, Cork, Ireland, pp. 161–164, 29Aug.–2Sept.2005. N. Barbour & G. Schmidt. *Inertial sensors technology trends*. IEEE Sensors Journal, vol. 1, no. 4, pages 332 – 339, Dec. 2001.